Optical Blood Flow Monitoring in Humans Using SNSPDs and High-Density SPAD Cameras

Carsi Kim[1], Christopher H. Moore[1], Chien-Sing Poon[2], Michael A. Wayne[4], Paul Mos[4], Arin Ulku[4], Timothy M. Rambo[3], Aaron J. Miller[3], Claudio Bruschini[4], Edoardo Charbon[4], and Ulas Sunar[1]
*ulas.sunar@stonybrook.edu

[1]*Dept of Biomedical Engineering, Stony Brook University, Stony Brook, NY, USA*
[2]*Dept of Biomedical Engineering, Wright State University, Dayton, OH, USA*
[3]*Quantum Opus LLC*
[4]*Advanced Quantum Architecture Laboratory, École polytechnique fédérale de Lausanne, Rue de la Maladière 71B, Neuchatel, NE 2000, Switzerland*

Abstract: Continuous and non-invasive monitoring of cerebral blood flow (CBF) is essential for managing acute brain injuries. Time-domain diffuse correlation spectroscopy (TD-DCS) enables depth-sensitive microvascular blood flow assessment using time-of-flight information in diffuse media like living tissue. This paper presents recent developments in TD-DCS using superconducting nanowire single-photon detectors (SNSPDs) and high-density single-photon avalanche diode (SPAD) arrays. We demonstrate improved signal-to-noise (SNR) and depth sensitivity at 1064 nm wavelengths using photon time-gating, and optimized instrument response functions. Experimental results from head-of-bed (HOB) and pressure modulation protocols validated the system's capability in isolating deeper cerebral signals. The additional assessment of SPAD-based detectors with preliminary hand grip and HOB protocols showed results complementing our CW-DCS system. This places the SPAD-based approach in a more advantageous position than traditional CW-DCS systems, especially in terms of SNR and scalability. With future enhancements such as fast time-gating and improved quantum efficiency, SPAD arrays can bridge the gap for implementing time-domain systems in clinical settings due to their sensitivity, compactness and cost-effective features. Similarly, SNSPD arrays can become a viable alternative or complement to SPAD arrays in TD-DCS, especially for deep-tissue imaging where performance near 1064 nm is desirable.

Index Terms: optical blood flow; time-domain diffuse correlation spectroscopy (TD-DCS); time-gating (TG), early and late gate; SPAD-based speckle imaging

Introduction

Acute brain injury, including traumatic brain injury (TBI), stroke, and subarachnoid hemorrhage (SAH), remains a leading cause of death and long-term disability. Effective clinical management in neurocritical care units (neuro-ICUs), require timely detection and intervention to prevent secondary brain injuries caused by cerebral ischemia (Vajkoczy et al., 2007). Similarly, in progressive neurological and neuromuscular disorders such as muscular dystrophies(Pomp et al., 2023) and Huntington's disease(Fathalizade & Ghaderyan, 2025), continuous physiological monitoring may aid in understanding disease progression and guiding diagnosis. In both cases, the need for non-invasive, real-time monitoring of blood flow and tissue function is critical. While blood flow assessments hold promises for revealing important physiological changes in neuromuscular conditions, they remain underutilized in routine monitoring. At the same time, existing neuromonitoring tools are either invasive, limited in temporal resolution, or insufficiently sensitive to deep brain tissue (Fantini et al., 2016). Conventional imaging modalities such as computed tomography (CT), magnetic resonance imaging (MRI), and positron emission tomography (PET) provide structural or metabolic information but are impractical for continuous bedside monitoring (Vajkoczy et al., 2007). Invasive methods, including intracranial pressure (ICP) probes and thermal diffusion flowmetry (TDF), offer direct cerebral blood flow (CBF) measurements but require burr hole placement and carry associated risks such as infection and hemorrhage (Fantini et al., 2016). Furthermore, these tools measure CBF in a very limited region and can suffer from intermittent data loss during calibration cycles.

Non-invasive approaches like near-infrared spectroscopy (NIRS) and transcranial Doppler ultrasound (TCD) offer partial insights into cerebral hemodynamics. However, NIRS is limited in sensitivity and cannot directly quantify CBF (Boas & Franceschini, 2011), while TCD is highly operator-dependent and restricted to large arteries (Y. Pan et al., 2022; Sharma et al., 2023). Continuous EEG (cEEG) provides valuable information about electrophysiological status and is increasingly used in neuro-ICUs, but its sensitivity to ischemic events is limited by low signal-to-noise ratio, interference from sedatives, and challenges in interpretation (Friedman et al., 2009).

Diffuse correlation spectroscopy (DCS) is an emerging optical technique that addresses many of these limitations. By measuring speckle intensity fluctuations from coherent near-infrared light, DCS enables continuous, non-invasive assessment of

microvascular blood flow (Boas et al., 1995; Boas & Yodh, 1997; Durduran et al., 2010; Mesquita et al., 2011). However, conventional continuous-wave DCS (CW-DCS) faces limitations in depth sensitivity, signal contamination from extracerebral tissues, and low signal-to-noise ratio (SNR) at longer source-detector separations (Baker et al., 2019; Forti et al., 2019; M. N. Kim et al., 2014; Mullen et al., 2019; Rowley, 2013) .

Recent advances in time-domain DCS (TD-DCS) provide a path toward overcoming these challenges. By tagging photons based on their time-of-flight (TOF), TD-DCS enables pathlength-resolved analysis that improves depth discrimination and sensitivity to CBF. Using longer wavelengths, such as 1064 nm, further enhances penetration and SNR due to reduced scattering and increased permissible laser power under ANSI safety guidelines (Carp et al., 2023). Integration of pulsed lasers, high-efficiency detectors, and time-correlated single-photon counting (TCSPC) hardware enables TD-DCS systems to be deployed in portable configurations suitable for bedside monitoring. Several studies have demonstrated the feasibility of TD-DCS for measuring CBF in vivo under physiologically relevant conditions, including controlled pressure modulation (Carp et al., 2023; Pagliazzi et al., 2017; Samaei et al., 2021) neurocritical care monitoring (Poon et al., 2022), and physical maneuvers such as Valsalva maneuver (Parfentyeva et al., 2023). In another vein, multi-speckle fast detectors like SPAD arrays have been utilized recently to improve the SNR of DCS. In addition to their photon-counting capabilities, SPAD array-based systems offer the potential for flexible, modular, and clinically adaptable optical neuro-monitoring platforms(Dragojević et al., 2016; Kreiss et al., 2025; Mata Pavia et al., 2014; M. A. Wayne et al., 2023). Currently SPAD arrays have been used in several blood flow applications (Murali & Varma, 2020)(Zhou et al., 2018),(Johansson et al., 2019),(Liu et al., 2021; Renna et al., 2022)(Xu et al., 2022),(Gorman et al., 2024; Kreiss et al., 2025; M. Wayne et al., 2022; M. A. Wayne et al., 2023),(M. Pan et al., 2025). Although the time-gating resolution in current SPAD devices is relatively coarse, some degree of pathlength sensitivity may still be achievable, albeit with certain limitations. This work presents several recent and new applications in TD-DCS, and SPAD-based approaches such as pressure modulation, head-of-bed manipulation, and hand-grip experiments.

Model for Tissue Blood Flow Index

When coherent light enters tissue, it undergoes multiple scattering events, where moving red blood cells (RBCs) result in temporal fluctuations in the detected speckle intensity. The temporal autocorrelation of these intensity fluctuations reflects the underlying blood flow dynamics(Boas et al., 1995; Boas & Yodh, 1997; Carp et al., 2020, 2023; Durduran & Yodh, 2014; Favilla et al., 2014; M. N. Kim et al., 2014; Li et al., 2017; Mesquita et al., 2011; Sakadžic et al., 2017; Sutin et al., 2016; Yu et al., 2011). The detected photon intensity autocorrelation function, $g_2(t_s,\tau)$, is defined as, $g_2(t_s,\tau) = < I(t_s,t)\, I(t_s,t+\tau) >_t / < I(t_s,t) >_t^2$,where t_s is the photon time-of-flight (TOF), or "micro-time", which is proportional to the photon pathlength through the medium, τ is the correlation delay (lag time), $<.>_t$ denotes averaging over macro-time , t, i.e., the absolute photon arrival time from the start of the measurement. In time-domain or time-gated DCS, this time-resolved autocorrelation function is typically modeled using the Siegert relation,$g_2(t_s,\tau) = 1 + \beta |\, g_1(t_s,\tau)|^2$,where g_1 is the normalized electric field autocorrelation function, which encodes information about scatterer motion, and β is the coherence factor. In the diffusion approximation, $g_1(s,\tau)$ is expressed as an integral over photon path lengths s, where s is the total optical path length traveled by the photon through the scattering medium, corresponding to its time-of-flight and related to the tissue geometry and scattering properties, and the model becomes$g_1(s,\tau) = \int P(s) \cdot \exp(-k_0^2 D_B \tau)\, ds$,where $P(s)$ is the photon path length distribution from the temporal point spread function (TPSF), D_B is the effective Brownian diffusion coefficient, and$k_0 = 2\pi n/\lambda$is the optical wavenumber with n being the index of refraction, and λ the wavelength. The blood flow index (BFI) is then estimated as αD_B where α is the fraction of dynamic scatterers. Unlike continuous-wave DCS, TD-DCS models g_2 as a function of pathlength-resolved photon dynamics, offering enhanced depth sensitivity and specificity to microvascular flow, as demonstrated before (Colombo et al., 2019, 2020; Li et al., 2017; Mazumder et al., 2021; Ozana, Zavriyev, et al., 2021; Parfentyeva et al., 2023; Sutin et al., 2016; Tamborini, 2019) and as below.

Instrumentation

A general fiber-based TD-DCS system is depicted in Fig.1(A). From left to right, TD-DCS begins with short, long coherence laser pulses. This laser's sync signal is coupled to a time-correlated single-photon counting (TCSPC) module where laser pulses can be correlated to detected photons. The laser is then sent through a multimode fiber into the tissue. Light is detected by a single mode fiber coupled to a single photon detector; currently the most common detectors used in TD-DCS are superconducting nanowire single-photon detectors (SNSPDs) or SPADs (Ozana, Zavriyev, et al., 2021; Poon et al., 2022). Next, a TCSPC module registers detected photons to timed laser pulses, generating a TPSF curve. From this TPSF curve different photon arrival time gates can be chosen based on the depth pathlength of interest. Photons arriving before the peak are referred to as early gate photons and signify photons that have penetrated shallower into the tissue. Photons arriving near the tail end of the peak are late gate photons and indicate deeper penetration due to longer photon arrival time. The information in the TPSF curve is then autocorrelated to calculate BFI, using either hardware or software components.

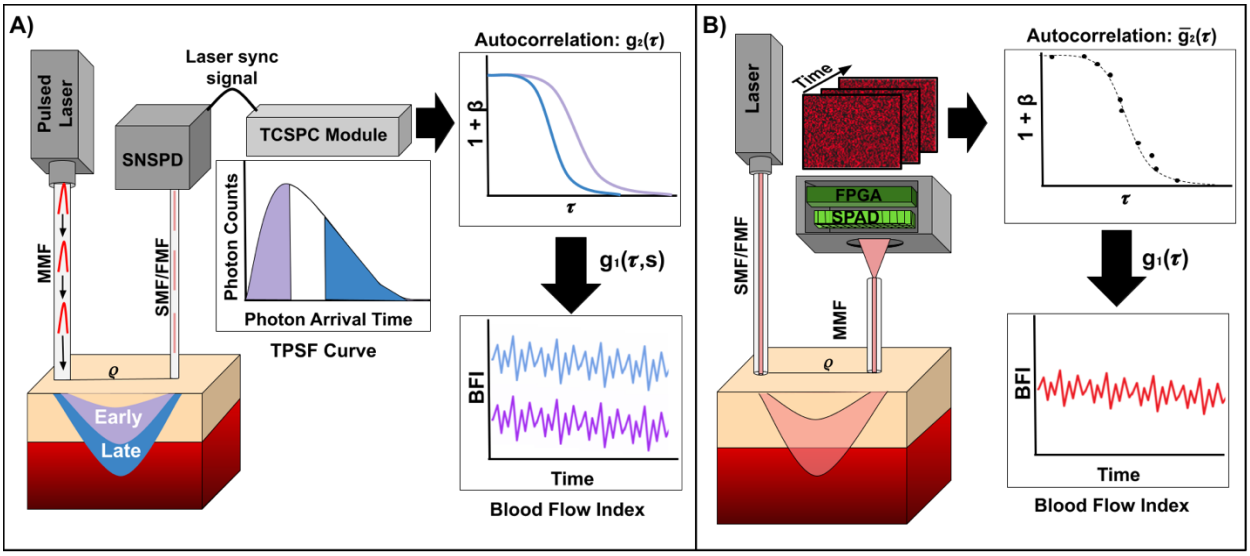

Figure 1. The schematic illustrates (A) TD-DCS and (B) SPAD-based multi-pixel DCS (mDCS) setups. (A) A pulsed laser delivers coherent light into tissue. The time-correlated single-photon counting (TCSPC) module records photon time-of-flight to generate a temporal point spread function (TPSF). Time-gating selects photons by arrival time-early (purple) and late (blue) gates. From these gated photons, the autocorrelation function is computed as a function of photon path lengths, s, to estimate the blood flow index (BFI). (B) The mDCS workflow using a SPAD array in continuous wave. "Each pixel" behaves as detector. Then the electric field autocorrelation is derived via the Siegert relation. The resulting g1(τ) is then fitted to a diffusion model to estimate the blood flow index (BFI)

A general SPAD-based DCS system is shown in Fig.1(B). In this setup, a coherent laser is delivered to the tissue via a single-mode or few-mode fiber (SMF/FMF). The scattered light is collected by a multimode fiber (MMF) and directed onto a SPAD array detector. The SPAD array captures multiple spatially independent speckle patterns in parallel. Each pixel detects individual photon events over time, enabling the tracking of dynamic speckles that change as red blood cells move within the tissue. The time-varying speckle patterns are then processed on an FPGA or through software to eventually calculate BFI (Dragojević et al., 2016; Kreiss et al., 2025; M. A. Wayne et al., 2023).

Detector Specifications: SNSPDs & SPAD Camera

The SNSPD detectors used for TD-DCS are a set of eight superconducting nanowire detectors from Quantum Opus with a cryostat cooling them to an operating temperature of ~2.5 K. These NIR-optimized detectors have a high detection efficiency of >80% at 1064 nm and low timing jitter of <80 ps(Quantum Opus, 2017). An amplifier unit couples to the readout of the detectors and generates standard TTL logic levels for our TCSPC module.

The SPAD camera array used for this study was a SwissSPAD3, which is a 500 x 500 binary, dual-gate CMOS SPAD array split into two 250 x 500 halves. Its readout is virtually noiseless, thanks to the direct in-pixel photon-to-digital conversion. This allows operation at very high frame rates with no penalty. Each half requires its own FPGA daughter board and only one half was used here. The camera has a pixel pitch of 16.38 µm with a SPAD active area of 6 µm diameter per pixel(M. Wayne et al., 2022). Each SPAD has a breakdown voltage of ~23 V and we operated our camera at 28 V for an excess bias voltage of ~5 V. At our operating wavelength of 785 nm this allows for a photon detection probability of ~13%. With the camera's maximum framerate of close to 100 kfps, the FPGA is able to calculate the autocorrelation with a minimum lag time of nearly 10-5 s(M. A. Wayne et al., 2023).

Validation: TD-DCS SNSPDs at 1064

First, to evaluate the feasibility of the TD-DCS system a Monte Carlo head model simulation was run at 785 nm comparing TD-DCS and CW-DCS. Then, to validate in-vivo applications of TD-DCS at 1064 nm multiple experiments were carried out and analyzed, such as transmission of a rat brain, head-of-bed protocol for multiple subjects, pressure modulation on the head, and clinical neuro-ICU patient monitoring. For future applications in the TD field, SPAD cameras are of interest. In this paper, only CW SPAD is analyzed. To assess the feasibility of CW SPAD a hand grip and HOB protocol were done in tandem with a CW DCS system. The International Review Board of Wright State University approved these protocols and participants consented to all measurements.

Increased Depth-Sensitivity via Time-Gating

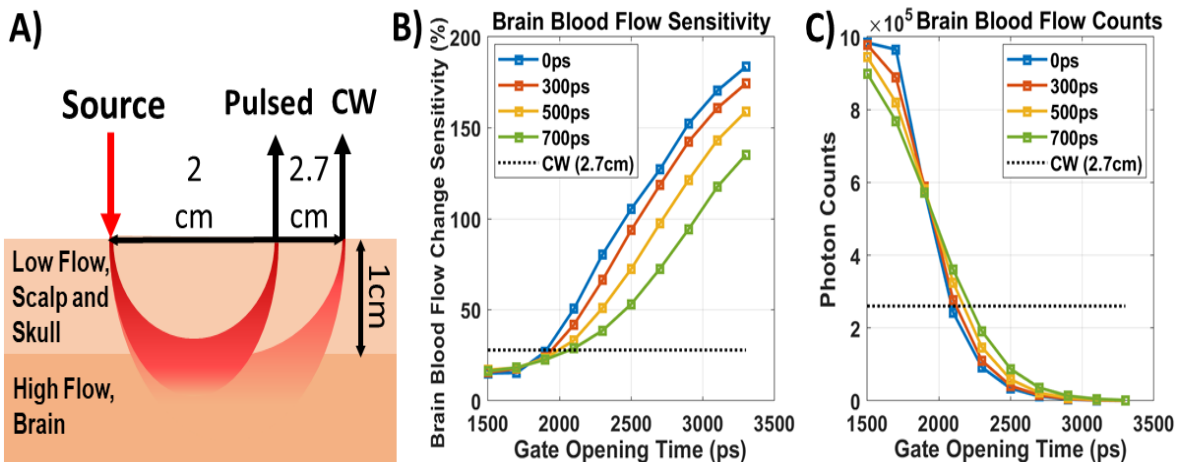

Figure 2. (A) The 2-layer brain model. (B) The brain blood flow changes sensitivity with increasing gate opening time starting from 1.5ns compared to CW, demonstrating significant sensitivity increase. (C) The number of counts at increasing gate opening time compared to CW

To demonstrate increased depth-sensitivity in time-gating measurements, we performed a Monte Carlo (MC) simulation of the gated pulse laser at 2 cm S-D separation and with the ungated (continuous wave (CW)) at 2.7 cm as a comparison, which is the maximum single detector distance used in DCS for brain measurements in humans (Ayaz et al., 2022). The top layer represents the scalp and skull optical properties with an absorption parameter of 0.154 cm-1, and scattering parameter of 7.9 cm-1, while the bottom layer or the brain layer has an absorption parameter of 0.186 cm-1, and scattering parameter of 11.1 cm-1 (Fig. 2A) (Carp et al., 2020; Li et al., 2017). The late-gated temporal point spread function (TPSF) is simulated by convoluting the tissue response to a Gaussian instrument response function (IRF) of different pulse width [0, 300, 500, 700] ps with the peak centered at 1500ps and a source-detector (S-D) separation of 2 cm. The late-gated TPSF is obtained by using only photons received after the gate opening time to increase the probability of obtaining photons that traveled into the brain layer. The ungated-DCS sensitivity is simulated by including all the photons detected at the S-D separation of 2.7 cm. The change in BFI sensitivity is calculated by taking the ratio between BFI at a baseline (1e-8cm2/s) for both layers and BFI (6e-8cm2/s) for the deeper layer.

Figure 2B clearly shows that there is a significant increase (>150%) in the cerebral blood flow index (CBFI) sensitivity of the gated-DCS as compared to the ungated-DCS at later gate opening times (>2.1ns). Figures 2B and 2C indicates that narrower pulses allow better sensitivity to the brain, while using wider pulses can still have better sensitivity than the ungated-DCS. We also plotted the decrease in photon counts due to the increasing gate opening time (Fig. 2C). The photon count level reaches the CW level around 2100ps. Thus, the time gated-DCS technique allows discriminating superficial blood flow and deeper blood flow, which is the key functionality in this approach that would positively impact overall sensitivity to deeper cerebral blood flow.

Increased Signal-to-Noise Ratio (SNR)

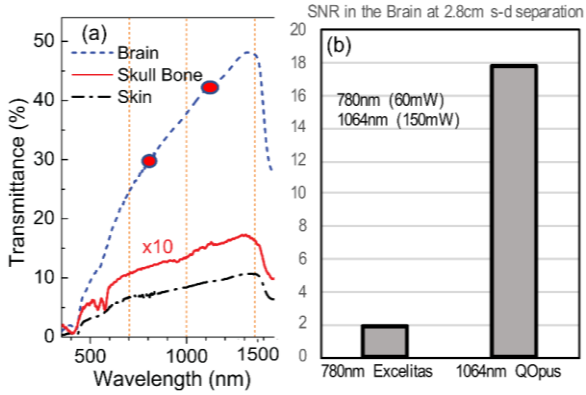

Figure 3. (A) Increased transmission in the rat brain with increasing wavelength. (B) Using 1064nm increases the SNR by more than 9x as compared to 780nm.

The reduced scattering coefficient (μs') of biological tissues decreases significantly with increasing wavelength, as predicted by the Mie scattering model [31–34]. This spectral behavior enables deeper light penetration and reduced photon scattering losses at longer wavelengths. Fig.3(A) shows the transmittance spectra for freshly harvested rat brain, cranial bone, and skin tissue(Golovynskyi et al., 2018). These data confirm that transmission increases with wavelength due to the reduction in scattering. However, while transmittance continues to rise beyond 1064 nm, water absorption also increases, limiting practical gains in SNR for human cerebral applications beyond this wavelength. As such, 1064 nm represents an optimal spectral region for deep cerebral imaging, balancing reduced scattering and manageable absorption. Accordingly, our system and those of other groups focus on this wavelength for optimal depth sensitivity(Carp et al., 2020; Colombo et al., 2020; Ozana, Peruch, et al., 2021; Poon et al., 2022).

Beyond wavelength selection, chosen detector fiber size and laser power further influence SNR. A key benefit of operating at 1064 nm is that it allows the use of larger-core detector fibers (e.g., 8.2 μm versus 4.5 μm) without excessive mode transmission, yielding approximately a ~4-fold increase in detected signal compared to smaller cores. Additionally, ANSI safety standards permit nearly three times greater laser power at SWIR wavelengths than in the NIR (Liu et al., 2021), further enhancing SNR without exceeding safe exposure limits. Together, these spectral and hardware considerations define a favorable design space for TD-DCS at 1064 nm. Improved photon throughput, reduced scattering, increased allowable power, and favorable fiber optics all contribute to enhanced SNR, which is particularly crucial for late-gated photon detection and depth-sensitive hemodynamic measurements.
In a direct comparison using superconducting nanowire single-photon detectors (SNSPDs), we observed a ~9-fold increase in detected signal at 1064 nm relative to 780 nm in the human brain, Fig.3(B). This substantial enhancement in photon detection is especially valuable in time-domain DCS, where late-arriving photons are sparse and critical for probing deeper tissues. The higher photon yield directly improves the signal-to-noise ratio (SNR), enabling more stable and higher-resolution blood flow measurements.

Human HOB Protocol using CW-DCS and SNSPDs

We first worked in CW-DCS mode for the HOB protocol to check the practical signal gain and feasibility of performing the experiments.

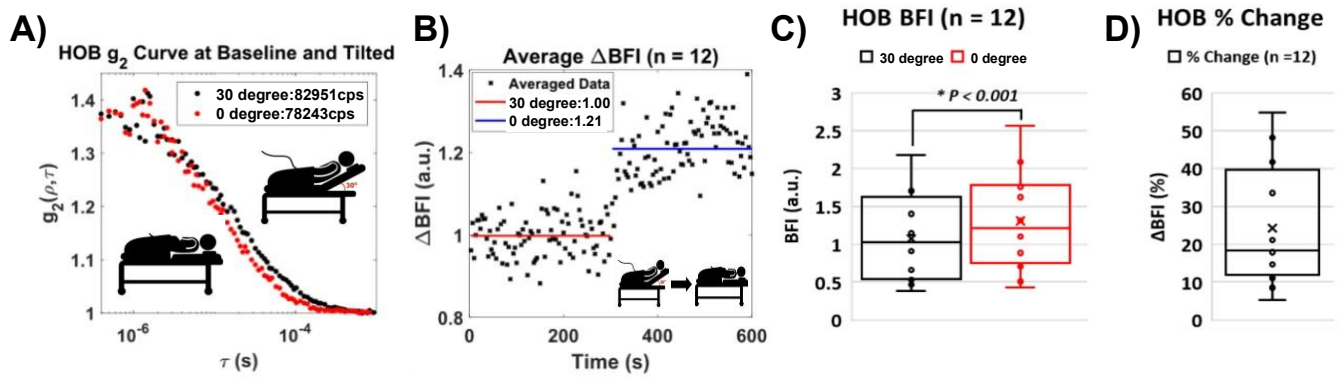

Figure 4. The head of bed (HOB) experiment is performed on 12 subjects. (A) A representative g2 curve between baseline, black, and tilted, red. (B) Data compared between the group average baseline and tilted cases and a significant difference was observed in the blood flow index (BFI) with a p<0.001 using rank sum test. (C) Comparison of average BFI during baseline and tilted. (D) Percent change of BFI when transitioning between baseline and tilted.

Twelve healthy subjects were recruited for the HOB protocol. The probe was placed on the prefrontal cortex of the subject. The subjects were told to rest on a hospital bed that is set to be flat. The 1064nm laser's fiber was placed on the subject's forehead between Fp1 and F7 of the EEG 10/20 system. The ~5μm single mode fiber was placed at 3cm away from the source and is connected to superconducting nanowire single-photon detectors (SNSPDs). Data was sampled at ~0.3Hz. The subject laid on a motorized hospital bed tilted 30 degrees up for 5 min to establish steady-state blood flow. After 5 minutes, the system will start collecting data for another 5 minutes in the same position, then the bed will drop to a 0-degree tilt, and the system will continue to collect for another 5 minutes. Fig.4(C), the comparison of CBFI between the group average baseline and tilted cases showed a ~(24.2±16.2)% increase, with a p-value of <0.001, using rank sum test. Fig.4(B) shows individual changes between baseline and tilted positions indicating large variations in the response, while Fig.4(A) shows a representative g2 curve between baseline and tilted case. These results align well with the previous HOB studies performed by CW-DCS at 785nm(Favilla et al., 2014; M. N. Kim et al., 2014), and that SNSPDs can reliably obtain CBF changes at 1064nm in humans in a clinically relevant protocol, with higher SNR and slightly longer source-detector separation (2.5cm vs 2.8 cm).

Pressure Modulation on the Head with TD-DCS and SNSPDs

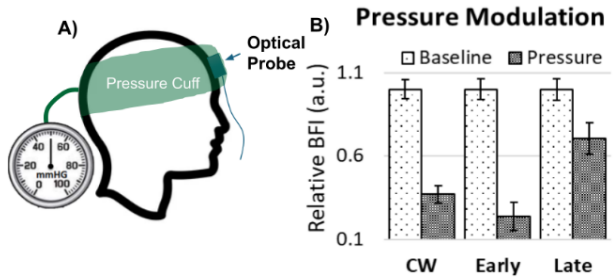

Figure 5. (A) Pressure modulation on scalp. Scalp is pressed hard (~50 mmHg) to reduce the blood flow in the scalp. (B) Late-gate (LG) photons show less change compared to continuous-wave (CW) and early-gate (EG) groups.

To validate our TD-DCS system we performed a typical pressure modulation on the head, and then a staged pressure modulation where pressure differences were set into timed increments (Baker et al., 2014; Carp et al., 2020; Colombo et al., 2020; Poon et al., 2022; Samaei et al., 2021; Tamborini, 2019). A typical protocol for TD-DCS has been pressure modulation, where the probe is pressed on the forehead to reduce blood flow seen from the superficial layer, predominantly the scalp (Fig. 5A). We performed pressure modulation on the scalp to occlude the scalp blood flow, by controlled pressure application (50mmHg) pressing the optical probe for 60s after a 60s baseline acquisition (Fig. 5A). CW and EG had higher changes (63%, 76%, respectively) vs 30% change in LG, as expected since LG photons has less sensitivity to scalp (Fig. 5B). Overall, these results show LG photons have high sensitivity to deeper flow.

Clinically relevant developments in SNSPD technology

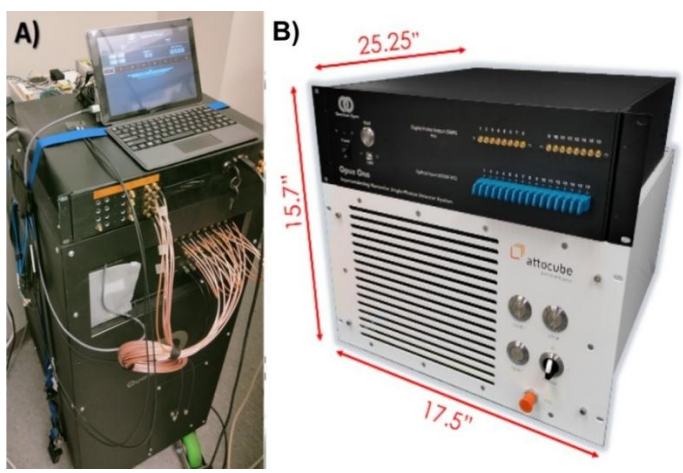

Figure 6. (A) Clinically translated version, 8-channel. (B) A complete 32-channel SNSPD system in a 7U rack mountable package using only commercial off-the-shelf components

The performance advantages of SNSPDs make them very useful diagnostic tools for a diverse array of applications. Additionally, due to its relative novelty, SNSPD technology is rapidly evolving, producing many clinically relevant improvements. These changes can be broadly separated into the categories of form factors, spectral response, and temporal characteristics.
The first clinical application of SNSPD-based TD-DCS was performed by Poon et al(Poon et al., 2022) (Fig. 6A). More compact versions, commercial SNSPD systems can support up to 32 detection channels (Fig. 6B). TD-DCS at 1064 nm was used in a case study for a patient with severe traumatic brain injury in a neuro-ICU setting. The IRF, TPSF, EG, LG, g2 curves, and
CBF were all measured or calculated. EG and LG BFI measurements were compared to invasive TDF. This comparison yielded strong correlations ($\rho = 0.67$ for early gate, $\rho = 0.76$ for late gate). Additionally, the TD-DCS system operated at a high sampling rate of 50 Hz, allowing for the observation of pulsatile blood flow dynamics. A zoomed-in segment of the high-resolution BFI trace shows clear rhythmic fluctuations (Fig.7D). The clinical events (sedation off, neurological exam, sedation resumed) further demonstrate the TD-DCS's sensitivity to physiological changes; this is all shown in Figure 7 (Ozana, Zavriyev, et al., 2021). This study represents the first successful clinical application of a TD-DCS system at 1064 nm using SNSPDs.

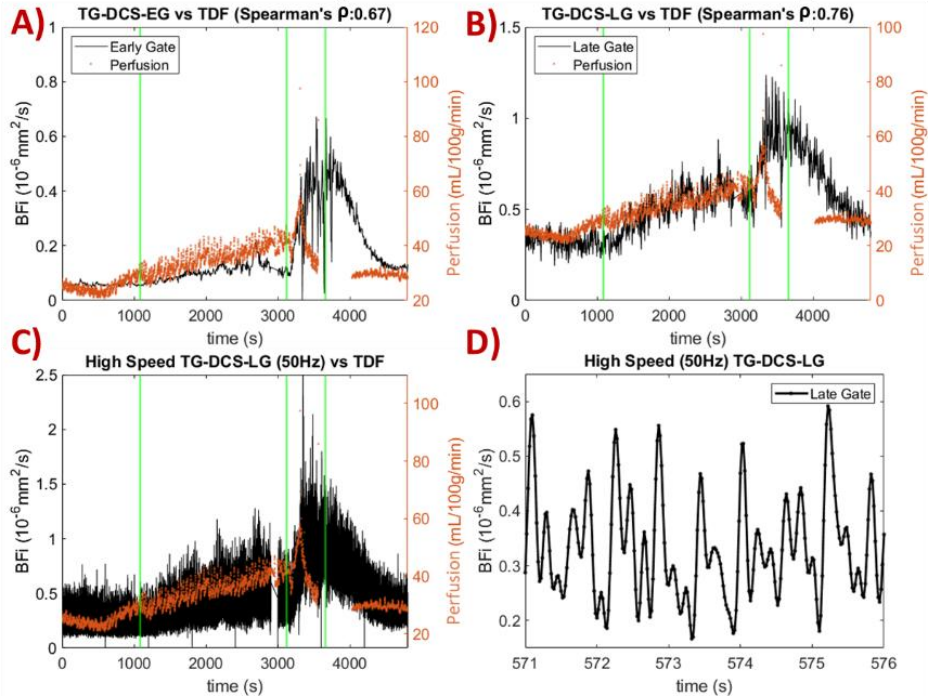

Figure 7: (A) Early-gated blood flow index (EG-BFI). (B) Late-gated BFI (LG-BFI) compared to invasive thermal diffusion flowmetry (TDF) cerebral blood flow (CBF), with Spearman's correlation coefficients of 0.67 and 0.76, respectively. (C) The 50 Hz LG-BFI signal captures distinct fluctuations associated with pulsatile blood flow. (D) A zoomed-in view of the 50 Hz BFI trace highlights pulsatility. The three green markers indicate key clinical events: (1) sedation stopped, (2) neurological exam performed, and (3) sedation resumed. Adapted from (Poon et al, 2022)(Poon et al., 2022).

While SNSPDs offer unsurpassed performance for many scientific applications, one key barrier to widespread adoption is that they require operation at cryogenic temperatures below 4 K. Pre-existing cryogenic technology can be packaged in a way that is roughly compatible with clinical settings, but the result is a somewhat bulky, noisy, power-hungry apparatus. New developments in commercial off-the-shelf cryogenic components can facilitate repackaging of the detectors into a significantly smaller, lower power, package, such as a 7U, all-in, fully-rack mountable SNSPD system with integrated vacuum pump and electronics(Rambo et al., 2024). By incorporating such a high number of channels into a significantly lower size, weight and power system, SNSPD DCS will be able to support a large number of measurement channels without imposing on the clinical environment.
Another key advantage of superconducting detectors is that the optical response of the films is incredibly broadband, ranging from UV(Wollman et al., 2017) to mid-infrared(Wollman et al., 2024) (Fig.8). While commercial SNSPDs were originally designed for near infrared and telecom wavelengths, they are now expanding through the visible spectrum and 2000 nm regimes. High performance detection at 2000 nm can allow for measurements with less scattering albeit higher absorption.

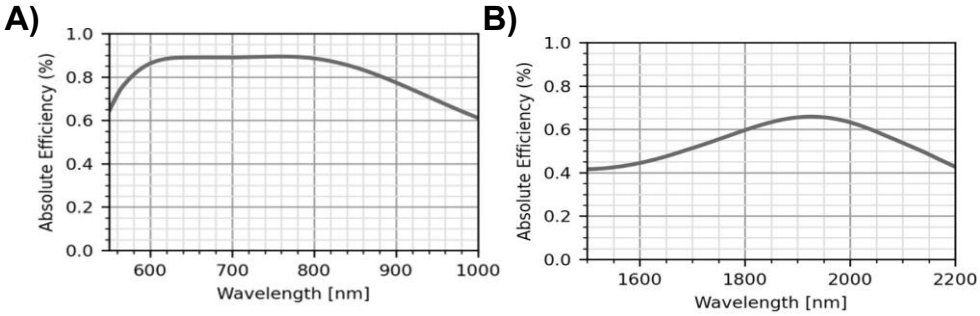

Figure 8. Typical detector performance curves reaching into the (A) visible, near infrared, and (B) infrared regimes

Furthermore, SNSPDs are seeing dramatic improvements in their temporal characteristics. They are counting faster and timing with better precision(Qin et al., 2024). After a detection event, the detector recovery is determined by the time dynamics of the bias current recharge in the detector structure, and in practice can allow single detector count rates of >100 MHz. This represents

roughly an order of magnitude improvement in count rate compared to conventional single-photon detectors, including SPADs and earlier SNSPD designs, potentially allowing for faster data acquisition, or operation at lower laser peak power with higher repetition rate lasers, potentially eliminating the need for optical amplifiers Current SNSPD implementations have been limited in terms of array size and pixel density. Recent breakthroughs, such as the development of a 400,000-pixel SNSPD camera by the NIST group, demonstrate a major step forward, offering a 400× improvement over previous kilopixel limits(Oripov et al., 2023).

Validation: High-Density SPAD-Array Based Time-Domain Blood Flow Measurements

To explore scalable detector alternatives to SNSPDs, others and our group have implemented a DCS system using a SPAD array in CW mode (Della Rocca et al., 2023; Fathi et al., 2025; Gorman et al., 2024; Kreiss et al., 2025; M. Pan et al., 2025; Wang et al., 2024; M. A. Wayne et al., 2023). Our SPAD camera, SwissSPAD3 (SS3) (Fig.9), fabricated in CMOS technology, operates without active gating, relying instead on post-processing the selected photon arrival windows for processing the (intensity). By integrating an advanced FPGA-based acquisition architecture, a ~500-fold improvement in signal-to-noise ratio (SNR) was achieved, compared to a conventional single-detector DCS system (M. A. Wayne et al., 2023). This high level of parallelization enables more sensitive detection within shorter acquisition times and creates new opportunities for capturing rapid physiological changes in deep tissue.

Figure 9: Image of the SwissSPAD3 (SS3) setup using one fiber and a 3D printed piece. The SS3 includes a daughterboard, motherboard, and a FPGA daughterboard. The SS3 daughterboard contains the main PCB where the SPAD array is. The motherboard includes the intermediate PCB, and the FPGA daughterboard contains the FPGA PCB.

Hand-grip Experiment

The primary response during handgrip exercise is increased blood flow in the exercising muscles. DCS measures relative blood flow index (rBFI), which reflects microvascular blood perfusion. This increase is due to local vasodilation in response to increase metabolic demand leading to an active hyperemia. Accumulation of metabolites like lactate and CO2 stimulates vasodilation, while sympathetic nervous system activity increases blood flow to active muscles while restricting flow to non-active areas. After the handgrip exercise stops, there is often a transient overshoot in blood flow (post-exercise hyperemia) before returning to baseline. This is caused by relieving mechanical compression of blood vessels squeezed during contraction and residual vasodilation from the need to restore oxygen levels and clear metabolic byproducts.

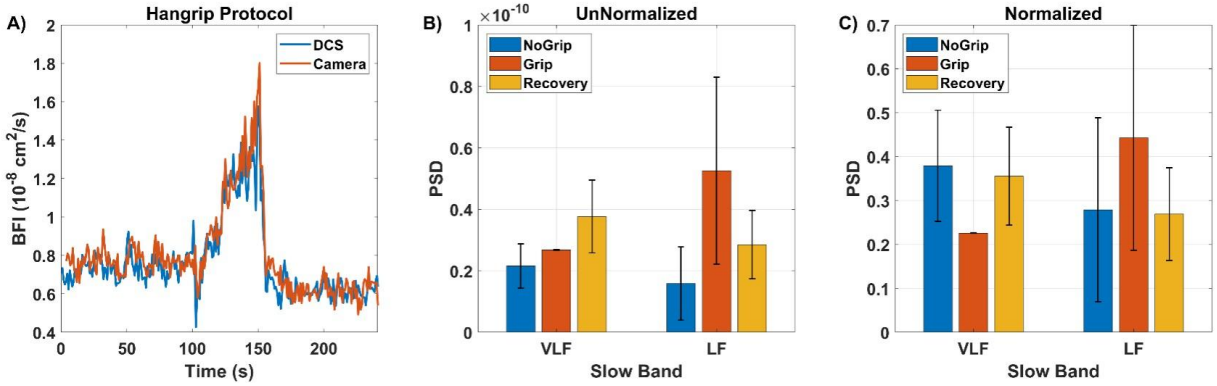

Figure 10: Data analysis for a hand grip protocol using mDCS: 100s relaxed, 60s grip, and 100s recovery relaxed. The probe was placed on the inner forearm and secured with velcro or adhesive wrap. (A) The blood flow index (BFI) plotted across time, seconds. CW-DCS is seen in blue, and the mDCS value are plotted in red. (B) Bar plot of very low frequencies (VLF) ranging from 0.02-0.07 Hz and LF ranging from 0.07 - 0.20 Hz. Standard deviation bars are plotted showing the variability of the PSD

frequencies in a LFO band. (C) Bar plot of very low frequencies (VLF) ranging from 0.02-0.07 Hz and LF ranging from 0.07 - 0.20 Hz. The data was normalized by the area under the power spectral density (PSD) curves. Standard deviation bars are plotted showing the variability of the PSD frequencies in a LFO band.

A hand grip protocol results for one healthy subject is shown in Figure 10. In Fig.10(A) the BFI time series of the hand grip shows the expected reaction of an increase in BFI during the gripping exercise and a drop after release. Importantly, the SPAD camera shows similar results to that of the CW DCS. In Fig.10(B) and (C) very low frequencies (VLF), 0.02-0.07, and low frequencies (LF), 0.07 - 0.20 Hz, are summed into bar plots. Error bars are calculated through standard deviation and reflect the variability of the PSD across the frequency band. The error bars are large due to the low frequency resolution. Fig.10(B) shows similar trends to existing similar muscle exercise BFI studies, where the exercise portion, grip, shows a higher PSD (Qin et al., 2024; Tarumi & Zhang, 2018). Fig.10(C) is the data normalized to the area under the PSD curve. Each curve is scaled so that the total power across all frequencies sums to one, which puts more of an emphasis on the relative distribution of power shifts across bands, rather than changes in total power. Fig 10.(B) focuses on absolute physiological responses while Fig.10(C) shows how the power is spread across different frequencies, which helps highlight changes in the shape of the signal rather than its overall strength.

While early LFO band definitions emerged from skin microcirculation studies, subsequent work has confirmed their presence and physiological relevance in skeletal muscle. In particular, Slow-3 reflects myogenic regulation of arteriolar tone during isometric contraction (Kindig & Poole, 1999), while Slow-4 and Slow-5 are modulated by neurogenic and endothelial factors during recovery (S. C. Kim et al., 2008; Zhang et al., 1998).

Head-of-Bed Protocol

A HOB protocol, like in the case of the DCS SNSPD system, was performed for the SPAD system but for different time durations. This experiment consisted of a healthy subject's data for a HOB protocol of 2 minutes supine and 2 minutes tilted upright for 30 degrees.

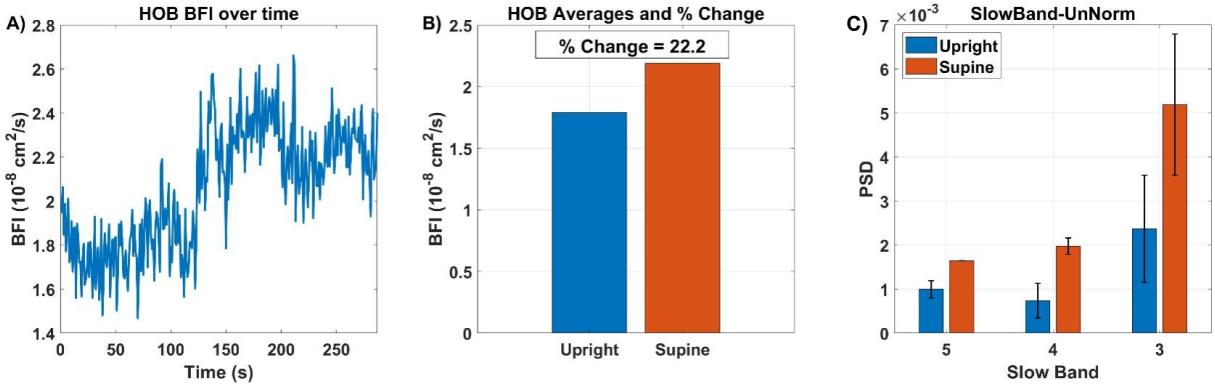

Figure 11: Data analysis for a head-of-bed protocol using mDCS at 2.5cm: 150s upright and 150s supine. The probe was placed on the forehead. (A) The blood flow index (BFI) plotted across time, seconds. (B) Average of the two baselines, upright and supine. The percent change between the two baselines was around 20%(C) The summed low frequency oscillation (LFO) PSD bands for slow band 5, 0.01 - 0.027 Hz, slow band 4, 0.027 - 0.073, and slow band 3, 0.073-0.198, for upright (blue) and supine (red). Standard deviation bars are plotted showing the variability of the PSD frequencies in a LFO band. Both PSD plots are normalized by the area under the power spectral density (PSD).

As seen in Fig 11.(A) is the BFI time series of the HOB protocol. The expected trend of increased BFI during the upright position is shown. The two baselines of upright and supine show an increase of about 20%. The HOB data taken with the SPAD system has a similar trend as the CW-DCS(1064 nm) system seen in Figure 6, and previously published results with traditional DCS at 785 nm(Favilla et al., 2014; M. N. Kim et al., 2014).

The difference between the supine and upright position can be indicator of systemic signal contamination, while we expect the change to be much higher in acute brain injury patients who usually have disrupted autoregulation.

These preliminary results demonstrate the viability of SPADs for TD-DCS and open a path toward compact, room-temperature, and potentially array-based optical imaging systems for blood flow measurements. Future work will explore optimization of timing electronics and photon selection strategies to further enhance performance.

Discussion and Outlook

This study presents advancements in the applications of TD-DCS for CBF monitoring using SNSPDs and SPAD array technologies. Our findings reinforce the use of time-gating for improved depth sensitivity while also showing clinically relevant implementations with significantly enhanced SNR, particularly at 1064 nm. Compared to 780 nm, there was a clear signal

enhancement at 1064 nm. This is advantageous in photon budgets and in measured permissible exposure. Through Monte Carlo simulations and in-vivo experiments, we showed that LG photons are substantially more sensitive to deeper cerebral layers compared to EG or CW approaches. This addresses a key limitation in CW-DCS, in which discriminating between cerebral and extracerebral signals is difficult.

The use of SNSPDs allows for high SNR and temporal resolution. In the HOB and pressure modulation experiments, we consistently observed robust BFI changes that aligned with physiological expectations and previous studies. Additionally, the strong correlation of LG BFI with invasive thermal diffusion flowmetry in a clinical case supports the validity and translational potential of our TD-DCS system. Although our SPAD-based system currently operates in CW mode, it offers promising potential for a scalable, modular TD system that can support broader applications. Recent progress in SPAD design further supports their future viability in TD-DCS systems particularly with the advancements in InGaAsP/InP SPADs with improved photon detection probability and low jitter at 1064 nm(Karaca et al., 2024). Our similarity in SPAD results to a CW-DCS system in a handgrip and HOB protocol demonstrates the feasibility of using mDCS derived from SPAD arrays to capture physiological changes.

A currently emerging approach is iDCS, which aims to achieve the same TOF abilities without the use of time-tagging electronics or cryogenic technology needed in SNSPDs. A current system in this field is PaLS-iDCS which has shown enhanced deep-tissue sensitivity and SNR by leveraging pathlength-specific coherent gain. This allows the system to have time-resolved blood flow measurements with improved depth selectivity all with a simplified instrument (Robinson, Renna, et al., 2024).Similarly, Zhao et al. demonstrated a scalable iDCS system with over 200 channels and electronically tunable coherence gating, which reduced scalp contamination and allowed TOF-resolved imaging (Zhao et al., 2023). Zhou et. al also validated functional iDWS improvements that rival current DCS techniques in brain specificity and throughput. This was done by using CMOS sensor arrays with coherent amplification(Zhou et al., 2021, 2022). These iDCS approaches can potentially address the cost, system bulk, and scalability issues in TD-DCS, while still preserving TOF sensitivity and clinical setting adaptability.

Although TD-DCS offers unique depth sensitivity, several practical limitations remain. A major challenge is developing lasers with both short pulse widths and long coherence lengths. A trade-off exists between spatial resolution, β, and signal strength, especially when increasing gate depth or optimizing detector geometry. High-performance detectors like SNSPDs offer low jitter and high efficiency, but their cost and cryogenic requirements hinder portability. Additionally, complex IRF calibration and variability in fiber and system design limit standardization. Addressing these challenges will be key to making TD-DCS more robust, compact, and clinically scalable.

While SPADs have enabled significant advances in time-resolved diffuse correlation spectroscopy (TD-DCS), especially in portable and scalable systems, SNSPDs offer complementary advantages that are increasingly relevant for high-performance TD-DCS and functional imaging for improved cerebral sensitivity at 1064nm. As SNSPDs provide exceptional performance metrics, near-unity quantum efficiency, sub-3 ps timing jitter, ultra-low dark count rates, and broad spectral sensitivity, large-format SNSPD arrays could become viable alternatives or complements to SPAD arrays in TD-DCS, especially for deep-tissue imaging where performance near 1064 nm is desirable. Further work is needed to evaluate the trade-offs in cryogenic complexity, integration, and cost, but SNSPD-based time-domain diffuse optics could provide unmatched performance in photon-starved conditions and unlock deeper imaging capabilities in neuroscience and neuroimaging applications.

Finally, we need to mention for another recent approach, although not time-domain, optical CMOS-based speckle contrast optical spectroscopy (SCOS) (Bi et al., 2013; B. Kim et al., 2023; Lin et al., 2023; Robinson, Cheng, et al., 2024; Valdes et al., 2014). Fast, high-resolution, and cost-effective CMOS cameras can track subtle changes in speckle patterns, allowing SCOS to measure blood flow non-invasively and practically with respect to cost, easy-to-use, and instrumentation. SCOS uses simpler and cheaper (but slower) cameras that allowed the development of multi-channel, high-density SCOS systems capable of mapping CBF changes over large cortical area with high spatial and temporal resolution(Cheng et al., 2024; (Kenny) Kim et al., 2025). Advancements in detection with fiber arrays, improved noise characterization, and parameter optimization have further enhanced measurement accuracy and accessibility. This makes SCOS a promising tool in noninvasive monitoring. Since the SPAD-based approach assesses g2 curves, it can be more sensitive to different scales (fast and slow) of blood flow and can provide quantitative blood flow metrics (assuming optical parameters are provided as a priori information), which may be required in several applications such as stroke and hydrocephalus where monitoring for absolute ischemia thresholds are important. A recent improvement in the SPAD camera by Henderson group (Gorman et al., 2024), implemented in 3D-stacked CMOS technology, has allowed a minimum autocorrelation lag-time of 1 μs, with having fill factor of 100% and maximum efficiency of ~50%, thereby providing human translation advantages.

Overall, future advances in optical neuro-monitoring will likely combine technologies like SPAD arrays, SNSPDs, and CMOS-based SCOS to meet specific needs. Multi-channel SNSPD systems offer unmatched sensitivity and temporal resolution for absolute and depth-resolved blood flow measurements, but they require cryogenic support. On the other hand, SPAD and CMOS systems allow for scalable and portable setups for relative flow monitoring. Rather than choosing one approach, hybrid systems could integrate these detectors into a setup balanced in depth sensitivity, spatial coverage, and practicality. This would support flexible, application specific designs optimized for clinical and research environments.

Acknowledgments

The authors acknowledge the funding support from NIH R01 (NIBIB Brain Initiative (7R01EB031759-03). We also thank Nick Bertone (Picoquant Inc.) for providing the demo unit of HydraHarp400 for the time domain acquisition system. M.W., P.M. and A.U. acknowledge partial support by the Swiss National Science Foundation (grants 20QT21_187716 Qu3D "Quantum 3D Imaging at high speed and high resolution" and 200021_166289). and in part by Meta Platforms Inc.

Disclosure

Edoardo Charbon is co-founder of Novoviz, and Claudio Bruschini and Edoardo Charbon are co-founders of Pi Imaging Technology. Neither company has been involved with the work or paper. The other authors declare that there are no conflicts of interest related to this article.

References

Ayaz, H., Baker, W. B., Blaney, G., Boas, D. A., Bortfeld, H., Brady, K., Brake, J., Brigadoi, S., Buckley, E. M., Carp, S. A., Cooper, R. J., Cowdrick, K. R., Culver, J. P., Dan, I., Dehghani, H., Devor, A., Durduran, T., Eggebrecht, A. T., Emberson, L. L., … Zhou, W. (2022). Optical imaging and spectroscopy for the study of the human brain: status report. *Neurophotonics*, *9*(S2). https://doi.org/10.1117/1.NPh.9.S2.S24001

Baker, W. B., Balu, R., He, L., Kavuri, V. C., Busch, D. R., Amendolia, O., Quattrone, F., Frangos, S., Maloney-Wilensky, E., Abramson, K., Mahanna Gabrielli, E., Yodh, A. G., & Andrew Kofke, W. (2019). Continuous non-invasive optical monitoring of cerebral blood flow and oxidative metabolism after acute brain injury. *Journal of Cerebral Blood Flow and Metabolism*, *39*(8), 1469–1485. https://doi.org/10.1177/0271678X19846657

Baker, W. B., Busch, D. R., Parthasarathy, A. B., Mesquita, R. C., Chandra, M., & Yodh, A. G. (2014). Probe Pressure Modulation Algorithm Reduces Extracerebral Contamination in Optical Measurements of Cerebral Blood Flow. *Biomedical Optics 2014*, BS3A.52. https://doi.org/10.1364/BIOMED.2014.BS3A.52

Bi, R., Dong, J., & Lee, K. (2013). Deep tissue flowmetry based on diffuse speckle contrast analysis. *Optics Letters*, *38*(9), 1401. https://doi.org/10.1364/OL.38.001401

Boas, D. A., Campbell, L. E., & Yodh, A. G. (1995). Scattering and Imaging with Diffusing Temporal Field Correlations. *Physical Review Letters*, *75*(9), 1855–1858. https://doi.org/10.1103/PhysRevLett.75.1855

Boas, D. A., & Franceschini, M. A. (2011). Haemoglobin oxygen saturation as a biomarker: the problem and a solution. *Philosophical Transactions of the Royal Society A: Mathematical, Physical and Engineering Sciences*, *369*(1955), 4407–4424. https://doi.org/10.1098/rsta.2011.0250

Boas, D. A., & Yodh, A. G. (1997). Spatially varying dynamical properties of turbid media probed with diffusing temporal light correlation. *Journal of the Optical Society of America A*, *14*(1), 192. https://doi.org/10.1364/JOSAA.14.000192

Carp, S. A., Robinson, M. B., & Franceschini, M. A. (2023). Diffuse correlation spectroscopy: current status and future outlook. *Neurophotonics*, *10*(01). https://doi.org/10.1117/1.nph.10.1.013509

Carp, S. A., Tamborini, D., Mazumder, D., Wu, K.-C. (Tony), Robinson, M. R., Stephens, K. A., Shatrovoy, O., Lue, N., Ozana, N., Blackwell, M. H., & Franceschini, M. A. (2020). Diffuse correlation spectroscopy measurements of blood flow using 1064 nm light. *Journal of Biomedical Optics*, *25*(09). https://doi.org/10.1117/1.jbo.25.9.097003

Cheng, T. Y., Kim, B., Zimmermann, B. B., Robinson, M. B., Renna, M., Carp, S. A., Franceschini, M. A., Boas, D. A., & Cheng, X. (2024). Choosing a camera and optimizing system parameters for speckle contrast optical spectroscopy. *Scientific Reports*, *14*(1), 11915. https://doi.org/10.1038/s41598-024-62106-y

Colombo, L., Pagliazzi, M., Konugolu Venkata Sekar, S., Contini, D., Durduran, T., & Pifferi, A. (2020). In vivo time-domain diffuse correlation spectroscopy above the water absorption peak. *Optics Letters*, *45*(13), 3377. https://doi.org/10.1364/OL.392355

Colombo, L., Pagliazzi, M., Sekar, S. K. V., Contini, D., Mora, A. D., Spinelli, L., Torricelli, A., Durduran, T., & Pifferi, A. (2019). Effects of the instrument response function and the gate width in time-domain diffuse correlation spectroscopy: model and validations. *Neurophotonics*, *6*(03), 1. https://doi.org/10.1117/1.NPh.6.3.035001

Della Rocca, F. M., Sie, E. J., Catoen, R., Marsili, F., & Henderson, R. K. (2023). Field programmable gate array compression for large array multispeckle diffuse correlation spectroscopy. *Journal of Biomedical Optics*, *28*(05). https://doi.org/10.1117/1.JBO.28.5.057001

Dragojević, T., Bronzi, D., Varma, H. M., Valdes, C. P., Castellvi, C., Villa, F., Tosi, A., Justicia, C., Zappa, F., & Durduran, T. (2016). A new method utilizing novel single-photon avalanche diode arrays for multi-exposure laser speckle flowmetry. *Biomedical Optics 2016*, JW3A.13. https://opg.optica.org/abstract.cfm?URI=BRAIN-2016-JW3A.13

Durduran, T., Choe, R., Baker, W. B., & Yodh, A. G. (2010). Diffuse optics for tissue monitoring and tomography. *Reports on Progress in Physics*, *73*(7), 076701. https://doi.org/10.1088/0034-4885/73/7/076701

Durduran, T., & Yodh, A. G. (2014). Diffuse correlation spectroscopy for non-invasive, micro-vascular cerebral blood flow measurement. *NeuroImage*, *85*, 51–63. https://doi.org/10.1016/j.neuroimage.2013.06.017

Fantini, S., Sassaroli, A., Tgavalekos, K. T., & Kornbluth, J. (2016). Cerebral blood flow and autoregulation: current measurement techniques and prospects for noninvasive optical methods. *Neurophotonics*, *3*(3), 031411. https://doi.org/10.1117/1.NPh.3.3.031411

Fathalizade, N., & Ghaderyan, P. (2025). An intelligent hemodynamic response analysis method to achieve prognosis and diagnosis of Huntington's disease. *Biocybernetics and Biomedical Engineering*, *45*(2), 287–295. https://doi.org/10.1016/j.bbe.2025.04.003

Fathi, F., Mazdeyasna, S., Singh, D., Huang, C., Mohtasebi, M., Liu, X., Rabienia Haratbar, S., Zhao, M., Chen, L., Can Ulku, A., Mos, P., Bruschini, C., Charbon, E., Chen, L., & Yu, G. (2025). Time-Resolved Laser Speckle Contrast Imaging (TR-LSCI) of Cerebral Blood Flow. *IEEE Transactions on Medical Imaging*, *44*(3), 1206–1217. https://doi.org/10.1109/TMI.2024.3486084

Favilla, C. G., Mesquita, R. C., Mullen, M., Durduran, T., Lu, X., Kim, M. N., Minkoff, D. L., Kasner, S. E., Greenberg, J. H., Yodh, A. G., & Detre, J. A. (2014). Optical Bedside Monitoring of Cerebral Blood Flow in Acute Ischemic Stroke Patients During Head-of-Bed Manipulation. *Stroke*, *45*(5), 1269–1274. https://doi.org/10.1161/STROKEAHA.113.004116

Forti, R. M., Favilla, C. G., Cochran, J. M., Baker, W. B., Detre, J. A., Kasner, S. E., Mullen, M. T., Messé, S. R., Kofke, W. A., Balu, R., Kung, D., Pukenas, B. A., Sedora-Roman, N. I., Hurst, R. W., Choudhri, O. A., Mesquita, R. C., & Yodh, A. G. (2019). Transcranial Optical Monitoring of Cerebral Hemodynamics in Acute Stroke Patients during Mechanical Thrombectomy. *Journal of Stroke and Cerebrovascular Diseases*, *28*(6), 1483–1494. https://doi.org/10.1016/j.jstrokecerebrovasdis.2019.03.019

Friedman, D., Claassen, J., & Hirsch, L. J. (2009). Continuous Electroencephalogram Monitoring in the Intensive Care Unit. *Anesthesia & Analgesia*, *109*(2), 506–523. https://doi.org/10.1213/ane.0b013e3181a9d8b5

Golovynskyi, S., Golovynska, I., Stepanova, L. I., Datsenko, O. I., Liu, L., Qu, J., & Ohulchanskyy, T. Y. (2018). Optical windows for head tissues in near-infrared and short-wave infrared regions: Approaching transcranial light applications. *Journal of Biophotonics*, *11*(12). https://doi.org/10.1002/jbio.201800141

Gorman, A., Finlayson, N., Erdogan, A. T., Fisher, L., Wang, Y., Mattioli Della Rocca, F., Mai, H., Sie, E. J., Marsili, F., & Henderson, R. K. (2024). ATLAS: a large array, on-chip compute SPAD camera for multispeckle diffuse correlation spectroscopy. *Biomedical Optics Express*, *15*(11), 6499. https://doi.org/10.1364/BOE.531416

Johansson, J. D., Portaluppi, D., Buttafava, M., & Villa, F. (2019). A multipixel diffuse correlation spectroscopy system based on a single photon avalanche diode array. *Journal of Biophotonics*, *12*(11). https://doi.org/10.1002/jbio.201900091

Karaca, U., Kizilkan, E., Bruschini, C., & Charbon, E. (2024). 10-µm InGaAsP/InP SPADs for 1064 nm detection with 36% PDP and 118 ps timing jitter. *2024 International SPAD Sensor Workshop (ISSW)*, *41*(16), R02.2.

(Kenny) Kim, B., Howard, A. C., Cheng, T. Y., Anderson, J. E., Zimmermann, B. B., Hazen, E., Carlton, L., Robinson, M., Renna, M., Yucel, M. A., Carp, S. A., Franceschini, M. A., Boas, D. A., & Cheng, X. (2025). Mapping human cerebral blood flow with high-density, multi-channel speckle contrast optical spectroscopy. *BioRxiv Preprint*, *10*. https://doi.org/10.1101/2025.03.03.638332

Kim, B., Zilpelwar, S., Sie, E. J., Marsili, F., Zimmermann, B., Boas, D. A., & Cheng, X. (2023). Measuring human cerebral blood flow and brain function with fiber-based speckle contrast optical spectroscopy system. *Communications Biology*, *6*(1), 844. https://doi.org/10.1038/s42003-023-05211-4

Kim, M. N., Edlow, B. L., Durduran, T., Frangos, S., Mesquita, R. C., Levine, J. M., Greenberg, J. H., Yodh, A. G., & Detre, J. A. (2014). Continuous optical monitoring of cerebral hemodynamics during head-of-bed manipulation in brain-injured adults. *Neurocritical Care*, *20*(3), 443–453. https://doi.org/10.1007/s12028-013-9849-7

Kim, S. C., Park, S. J., Lee, J. R., Seo, J. C., Yang, C. H., & Byun, S. H. (2008). Cytoprotective Activity of *Glycyrrhizae radix* Extract against Arsenite-Induced Cytotoxicity. *Evidence-Based Complementary and Alternative Medicine*, *5*(2), 165–171. https://doi.org/10.1093/ecam/nem014

Kindig, C. A., & Poole, D. C. (1999). Effects of Skeletal Muscle Sarcomere Length onin VivoCapillary Distensibility. *Microvascular Research*, *57*(2), 144–152. https://doi.org/10.1006/mvre.1998.2123

Kreiss, L., Wu, M., Wayne, M., Xu, S., McKee, P., Dwamena, D., Kim, K., Lee, K. C., Cowdrick, K. R., Liu, W., Ülkü, A., Harfouche, M., Yang, X., Cook, C., Lee, S. A., Buckley, E., Bruschini, C., Charbon, E., Huettel, S., & Horstmeyer, R. (2025). Beneath the surface: revealing deep-tissue blood flow in human subjects with massively parallelized diffuse correlation spectroscopy. *Neurophotonics*, *12*(02). https://doi.org/10.1117/1.NPh.12.2.025007

Li, J., Qiu, L., Poon, C.-S., & Sunar, U. (2017). Analytical models for time-domain diffuse correlation spectroscopy for multi-layer and heterogeneous turbid media. *Biomedical Optics Express*, *8*(12), 5518. https://doi.org/10.1364/boe.8.005518

Lin, C.-H. P., Orukari, I., Tracy, C., Frisk, L. K., Verma, M., Chetia, S., Durduran, T., Trobaugh, J. W., & Culver, J. P. (2023). Multi-mode fiber-based speckle contrast optical spectroscopy: analysis of speckle statistics. *Optics Letters*, *48*(6), 1427. https://doi.org/10.1364/OL.478956

Liu, W., Qian, R., Xu, S., Chandra Konda, P., Jönsson, J., Harfouche, M., Borycki, D., Cooke, C., Berrocal, E., Dai, Q., Wang, H., & Horstmeyer, R. (2021). Fast and sensitive diffuse correlation spectroscopy with highly parallelized single photon detection. *APL Photonics*, *6*(2). https://doi.org/10.1063/5.0031225

Mata Pavia, J., Wolf, M., & Charbon, E. (2014). Single-Photon Avalanche Diode Imagers Applied to Near-Infrared Imaging. *IEEE Journal of Selected Topics in Quantum Electronics*, *20*(6), 291–298. https://doi.org/10.1109/JSTQE.2014.2313983

Mazumder, D., Wu, M. M., Ozana, N., Tamborini, D., Franceschini, M. A., & Carp, S. A. (2021). Optimization of time domain diffuse correlation spectroscopy parameters for measuring brain blood flow. *Neurophotonics*, *8*(03), 35005. https://doi.org/10.1117/1.nph.8.3.035005.

Mesquita, R. C., Durduran, T., Yu, G., Buckley, E. M., Kim, M. N., Zhou, C., Choe, R., Sunar, U., & Yodh, A. G. (2011). Direct measurement of tissue blood flow and metabolism with diffuse optics. *Philosophical Transactions of the Royal Society A: Mathematical, Physical and Engineering Sciences*, *369*(1955), 4390–4406. https://doi.org/10.1098/rsta.2011.0232

Mullen, M. T., Parthasarathy, A. B., Zandieh, A., Baker, W. B., Mesquita, R. C., Loomis, C., Torres, J., Guo, W., Favilla, C. G., Messé, S. R., Yodh, A. G., Detre, J. A., & Kasner, S. E. (2019). Cerebral Blood Flow Response During Bolus Normal Saline Infusion After Ischemic Stroke. *Journal of Stroke and Cerebrovascular Diseases*, *28*(11), 104294. https://doi.org/10.1016/j.jstrokecerebrovasdis.2019.07.010

Murali, K., & Varma, H. M. (2020). Multi-speckle diffuse correlation spectroscopy to measure cerebral blood flow. *Biomedical Optics Express*, *11*(11), 6699. https://doi.org/10.1364/BOE.401702

Oripov, B. G., Rampini, D. S., Allmaras, J., Shaw, M. D., Nam, S. W., Korzh, B., & McCaughan, A. N. (2023). A superconducting nanowire single-photon camera with 400,000 pixels. *Nature*, *622*(7984), 730–734. https://doi.org/10.1038/s41586-023-06550-2

Ozana, N., Peruch, A., Robinson, M. B., Mazumder, D., Blackwell, M., Lue, N., Carp, S., & Franceschini, M. A. (2021). Time-gated diffuse correlation spectroscopy for functional imaging via 1064 nm pulse laser shaping and superconducting nanowire single photon sensing. In Q. Luo, J. Ding, & L. Fu (Eds.), *Optical Techniques in Neurosurgery, Neurophotonics, and Optogenetics* (p. 64). SPIE. https://doi.org/10.1117/12.2578909

Ozana, N., Zavriyev, A. I., Mazumder, D., Robinson, M., Kaya, K., Blackwell, M., Carp, S. A., & Franceschini, M. A. (2021). Superconducting nanowire single-photon sensing of cerebral blood flow. *Neurophotonics*, *8*(03). https://doi.org/10.1117/1.NPh.8.3.035006

Pagliazzi, M., Sekar, S. K. V., Colombo, L., Martinenghi, E., Minnema, J., Erdmann, R., Contini, D., Mora, A. D., Torricelli, A., Pifferi, A., & Durduran, T. (2017). Time domain diffuse correlation spectroscopy with a high coherence pulsed source: in vivo and phantom results. *Biomedical Optics Express*, *8*(11), 5311. https://doi.org/10.1364/BOE.8.005311

Pan, M., Li, C., Zhang, Y., Mollins, A., Wang, Q., Erdogan, A. T., Hua, Y., Zang, Z., Finlayson, N., Henderson, R. K., & Li, D. D.-U. (2025). Cerebral blood flow monitoring using a deep learning implementation of the two-layer DCS analytical model with a 512x512 SPAD array. *ArXiv Preprint*. http://arxiv.org/abs/2504.06997

Pan, Y., Wan, W., Xiang, M., & Guan, Y. (2022). Transcranial Doppler Ultrasonography as a Diagnostic Tool for Cerebrovascular Disorders. *Frontiers in Human Neuroscience*, *16*. https://doi.org/10.3389/fnhum.2022.841809

Parfentyeva, V., Colombo, L., Lanka, P., Pagliazzi, M., Brodu, A., Noordzij, N., Kolarczik, M., Dalla Mora, A., Re, R., Contini, D., Torricelli, A., Durduran, T., & Pifferi, A. (2023). Fast time-domain diffuse correlation spectroscopy with superconducting nanowire single-photon detector: system validation and in vivo results. *Scientific Reports*, *13*(1), 11982. https://doi.org/10.1038/s41598-023-39281-5

Pomp, L., Jeneson, J. A. L., van der Pol, W. L., & Bartels, B. (2023). Electrophysiological and Imaging Biomarkers to Evaluate Exercise Training in Patients with Neuromuscular Disease: A Systematic Review. *Journal of Clinical Medicine*, *12*(21), 6834. https://doi.org/10.3390/jcm12216834

Poon, C.-S., Langri, D. S., Rinehart, B., Rambo, T. M., Miller, A. J., Foreman, B., & Sunar, U. (2022). First-in-clinical application of a time-gated diffuse correlation spectroscopy system at 1064 nm using superconducting nanowire single photon detectors in a neuro intensive care unit. *Biomedical Optics Express*, *13*(3), 1344. https://doi.org/10.1364/BOE.448135

Qin, W., Fukuie, M., Hoshi, D., Mori, S., Tomoto, T., Sugawara, J., & Tarumi, T. (2024). Dynamic cerebral autoregulation during repeated handgrip exercise: comparisons with spontaneous rest and sit-stand maneuvers. *Journal of Applied Physiology*, *137*(3), 718–727. https://doi.org/10.1152/japplphysiol.00217.2024

Quantum Opus, L. (2017). *Superconducting Nanowire Single-Photon Detectors Datasheet*. https://quantumopus.com

Rambo, T., Doredla, J., Jones, H., Oshiro, L., Conover, A. R., Boyd, S., & Miller, A. J. (2024). New frontiers for commercial SNSPDs. In M. A. Itzler, K. A. McIntosh, & J. C. Bienfang (Eds.), *Advanced Photon Counting Techniques XVIII* (p. 6). SPIE. https://doi.org/10.1117/12.3015930

Renna, M., Richardson, J. M., Jordy, G., Cheng, T., Ringdahl, E., Robinson, M., Ozana, N., Lue, N., Aull, B., Carp, S., Duerr, E., Franceschini, M. A., & Blackwell, M. (2022). A novel 32x32 InP/ InGaAs SPAD array for multi-channel time-gated diffuse correlation spectroscopy. In M. A. Itzler, K. A. McIntosh, & J. C. Bienfang (Eds.), *Advanced Photon Counting Techniques XVI* (Vol. PC12089, p. 24). SPIE. https://doi.org/10.1117/12.2619112

Robinson, M. B., Cheng, T. Y., Renna, M., Wu, M. M., Kim, B., Cheng, X., Boas, D. A., Franceschini, M. A., & Carp, S. A. (2024). Comparing the performance potential of speckle contrast optical spectroscopy and diffuse correlation spectroscopy

for cerebral blood flow monitoring using Monte Carlo simulations in realistic head geometries. *Neurophotonics*, *11*(01). https://doi.org/10.1117/1.NPh.11.1.015004

Robinson, M. B., Renna, M., Otic, N., Kierul, O. S., Muldoon, A., Franceschini, M. A., & Carp, S. A. (2024). Pathlength-selective, interferometric diffuse correlation spectroscopy. *bioRxiv preprint*, *27*. https://doi.org/10.1101/2024.06.21.600096

Rowley, H. A. (2013). The alphabet of imaging in acute stroke does it spell improved selection and outcome? *Stroke*, *44*(SUPPL. 1). https://doi.org/10.1161/STROKEAHA

Sakadžic, S., Boas, D. A., & Carp, S. A. (2017). Theoretical model of blood flow measurement by diffuse correlation spectroscopy. *Journal of Biomedical Optics*, *22*(2), 027006. https://doi.org/10.1117/1.JBO.22.2.027006

Samaei, S., Sawosz, P., Kacprzak, M., Pastuszak, Ż., Borycki, D., & Liebert, A. (2021). Time-domain diffuse correlation spectroscopy (TD-DCS) for noninvasive, depth-dependent blood flow quantification in human tissue in vivo. *Scientific Reports*, *11*(1), 1817. https://doi.org/10.1038/s41598-021-81448-5

Sharma, R., Tsikvadze, M., Peel, J., Howard, L., Kapoor, N., & Freeman, W. D. (2023). Multimodal monitoring: practical recommendations (dos and don'ts) in challenging situations and uncertainty. *Frontiers in Neurology*, *14*. https://doi.org/10.3389/fneur.2023.1135406

Sutin, J., Zimmerman, B., Tyulmankov, D., Tamborini, D., Wu, K. C., Selb, J., Gulinatti, A., Rech, I., Tosi, A., Boas, D. A., & Franceschini, M. A. (2016). Time-domain diffuse correlation spectroscopy. *Optica*, *3*(9), 1006. https://doi.org/10.1364/OPTICA.3.001006

Tamborini, D. (2019). Portable System for Time-Domain Diffuse Correlation Spectroscopy. *IEEE Trans Biomed Eng*. https://doi.org/10.1109/TBME.2019.2899762.

Tarumi, T., & Zhang, R. (2018). Cerebral blood flow in normal aging adults: cardiovascular determinants, clinical implications, and aerobic fitness. *Journal of Neurochemistry*, *144*(5), 595–608. https://doi.org/10.1111/jnc.14234

Vajkoczy, P., Schomacher, M., Czabanka, M., & Horn, P. (2007). Monitoring Cerebral Blood Flow in Neurosurgical Intensive Care. *European Neurological Review*, *2*, 6. https://doi.org/10.17925/ENR.2007.00.02.6

Valdes, C. P., Varma, H. M., Kristoffersen, A. K., Dragojevic, T., Culver, J. P., & Durduran, T. (2014). Speckle contrast optical spectroscopy, a non-invasive, diffuse optical method for measuring microvascular blood flow in tissue. *Biomed Opt Express*, *5*(8). https://doi.org/10.1364/boe.5.002769.

Wang, Q., Pan, M., Kreiss, L., Samaei, S., Carp, S. A., Johansson, J. D., Zhang, Y., Wu, M., Horstmeyer, R., Diop, M., & Li, D. D. U. (2024). A comprehensive overview of diffuse correlation spectroscopy: Theoretical framework, recent advances in hardware, analysis, and applications. *NeuroImage*, *298*. https://doi.org/10.1016/j.neuroimage.2024.120793

Wayne, M. A., Sie, E. J., Ulku, A. C., Mos, P., Ardelean, A., Marsili, F., Bruschini, C., & Charbon, E. (2023). Massively parallel, real-time multispeckle diffuse correlation spectroscopy using a 500 × 500 SPAD camera. *Biomedical Optics Express*, *14*(2), 703. https://doi.org/10.1364/BOE.473992

Wayne, M., Ulku, A., Ardelean, A., Mos, P., Bruschini, C., & Charbon, E. (2022). A 500 × 500 Dual-Gate SPAD Imager with 100% Temporal Aperture and 1 ns Minimum Gate Length for FLIM and Phasor Imaging Applications. *IEEE Transactions on Electron Devices*, *69*(6), 2865–2872. https://doi.org/10.1109/TED.2022.3168249

Wollman, E. E., Taylor, G., Patel, S., Bumble, B., Korzh, B., Colangelo, M., Paul, D. J., Berkel, S. van, Walter, A., Allmara, J., Hampel, B., Berggren, K., & Shaw, M. (2024). Current state of mid-infrared superconducting nanowire single-photon detectors. In A. D. Holland & K. Minoglou (Eds.), *SPIE PC13103, X-Ray, Optical, and Infrared Detectors for Astronomy XI* (p. 1310306). https://doi.org/10.1117/12.3019299

Wollman, E. E., Verma, V. B., Beyer, A. D., Briggs, R. M., Korzh, B., Allmaras, J. P., Marsili, F., Lita, A. E., Mirin, R. P., Nam, S. W., & Shaw, M. D. (2017). UV superconducting nanowire single-photon detectors with high efficiency, low noise, and 4 K operating temperature. *Optics Express*, *25*(22), 26792. https://doi.org/10.1364/OE.25.026792

Xu, S., Liu, W., Yang, X., Jönsson, J., Qian, R., McKee, P., Kim, K., Konda, P. C., Zhou, K. C., Kreiß, L., Wang, H., Berrocal, E., Huettel, S. A., & Horstmeyer, R. (2022). Transient Motion Classification Through Turbid Volumes via Parallelized Single-Photon Detection and Deep Contrastive Embedding. *Frontiers in Neuroscience*, *16*. https://doi.org/10.3389/fnins.2022.908770

Yu, G., Durduran, T., Zhou, C., Cheng, R., & Yodh, A. G. (2011). Near-Infrared Diffuse Correlation Spectroscopy for Assessment of Tissue Blood Flow. In *Handbook of Biomedical Optics* (pp. 195–216). CRC Press.

Zhang, R., Zuckerman, J. H., Giller, C. A., & Levine, B. D. (1998). Transfer function analysis of dynamic cerebral autoregulation in humans. *American Journal of Physiology-Heart and Circulatory Physiology*, *274*(1), H233–H241. https://doi.org/10.1152/ajpheart.1998.274.1.H233

Zhao, H., Sathialingam, E., Cowdrick, K. R., Urner, T., Lee, S. Y., Bai, S., Akbik, F., Samuels, O. B., Kandiah, P., Sadan, O., & Buckley, E. M. (2023). Comparison of diffuse correlation spectroscopy analytical models for measuring cerebral blood flow in adults. *Journal of Biomedical Optics*, *28*(12). https://doi.org/10.1117/1.JBO.28.12.126005

Zhou, W., Kholiqov, O., Chong, S. P., & Srinivasan, V. J. (2018). Highly parallel, interferometric diffusing wave spectroscopy for monitoring cerebral blood flow dynamics. *Optica*, *5*(5), 518. https://doi.org/10.1364/OPTICA.5.000518

Zhou, W., Kholiqov, O., Zhu, J., Zhao, M., Zimmermann, L. L., Martin, R. M., Lyeth, B. G., & Srinivasan, V. J. (2021). Functional interferometric diffusing wave spectroscopy of the human brain. *Science Advances*, *7*(20). https://doi.org/10.1126/sciadv.abe0150

Zhou, W., Zhao, M., & Srinivasan, V. J. (2022). Interferometric diffuse optics: recent advances and future outlook. *Neurophotonics*, *10*(01). https://doi.org/10.1117/1.NPh.10.1.013502